Appendix C–SR-72 Tests

Table of Contents

C.1 Introduction 170
C.2 Girder and Deck Design 173
C.3 Test Setup, Procedures, and Instrumentation 176
C.4 Results and Discussion 180
C.4.1 Non-destructive testing to locate transverse reinforcement 180
C.4.2 Test X7 181
C.4.3 Test X4 184
C.4.4 I2A-Determination of Effective Prestress 190
C.4.5 Test I2A 192
C.4.6 Test I2B 195
C.4.7 Test I4 197
C.4.8 Test I6 199
C.5 Comparison with computed strength 202
C.6 Summary and Conclusions 206

List of Figures

Figure 1–Existing bridge prior to girder removal 170
Figure 2–Test girder identifications and slab configurations 172
Figure 3–Typical girder cross section 173
Figure 4–Transverse reinforcement 174
Figure 5–Deck and curb reinforcement 175
Figure 6–Test setup 176
Figure 7–LVDTs at end of girder 177
Figure 8–Strands instrumented with LVDTs 177
Figure 9–X7 far support 178
Figure 10–X4 far support 178
Figure 11–I6 far support 179
Figure 12–X7 shear vs. vertical displacement 181
Figure 13–X7 lateral displacement at load point 182
Figure 14–X7 cracks (initial crack in red) 183
Figure 15–X7 rosette R7 183
Figure 16–X7 punching failure bottom view 184
Figure 17–X7 Strain contour at shear of 45 kip at section below load point 184
Figure 18–X4 shear vs. displacement 185
Figure 19–X4 lateral displacement 185
Figure 20–X4 cracks (initial cracks in red) 186
Figure 21–X4 shear vs. strain S25 187
Figure 22–X4 strain field at load location at a superimposed shear of 46 kip 188
Figure 23–X4 shear vs. compressive strain 189
Figure 24–X4 strand slip vs. shear 189
Figure 25–I2A decompression gages 191
Figure 26–I2A load vs. decompression strain (crack opening) 191
Figure 27–I2A shear vs. displacement 193
Figure 28–I2A cracks (initial cracks in red) 193
Figure 29–I2A incline cracks in web 194
Figure 30–I2A transverse reinforcement-arch failure 194
Figure 31–I2A shear vs. strain S1 195
Figure 32–I2B superimposed shear vs. displacement 196
Figure 33–I2B crack pattern (initial cracks in red) 197
Figure 34–I4 shear vs. displacement 198
Figure 35–I4 principal strain vs. shear 198
Figure 36–I4 cracks (initial crack in red) 199
Figure 37–I6 shear vs. displacement. 200
Figure 38–I6 gage S29 vs. shear. 200
Figure 39–I6 cracks (initial crack in red). 201
Figure 40–Experimental and theoretical shear capacities. 203
Figure 41–Shear at initial cracking and theoretical concrete contribution 204

List of Tables

Table 1–Test setup dimensions 176
Table 2–I2A specified and effective prestress force 191
Table 3–Comparison of experimental and theoretical shear capacities. 203
Table 4–Exterior girder shear strength considering contribution of barrier 203
Table 5–Comparison of experimental and theoretical cracking shears 205
Table 6–Comparison of experimental moments and nominal moment capacities 205

1 Introduction

The Florida highway system includes some of the earliest (circa 1950s) pretensioned concrete bridges in the United States. Shear capacity of Florida's early pretensioned girders is of interest because the early designs had thin webs and only limited vertical reinforcement. This report presents the results of load testing conducted on early girders that were removed from an existing bridge (Figure 1) after nearly 55 years of service. In total, six girders were removed and tested. Girders were loaded in three-point bending at a/d ratios ranging from 2.1 to 4.5. Results of load testing will assist engineers in determining the strength of similar existing girders.

In addition to evaluating shear capacity of early pretensioned girders, this project also had the goal of evaluating the contribution to the shear capacity from the cast-in-place concrete bridge decks. To this end, varying portions of the deck and curb were retained with each salvaged test girder. Width of the retained deck portions ranged from 2 ft to 7 ft. Two of the girders were exterior girders and were removed with the curb portion of the bridge deck intact. The exterior girders allowed the strength and stiffness contributions of the curb to be evaluated.

Figure 1–Existing bridge prior to girder removal

Each girder was given a unique label based width of the retained deck and position as an internal or external girder (Figure 2). Internal girders were labeled with an 'I' and exterior girders with an 'X'. The numeric portion of each label indicates the nominal width of the slab in feel. For example, girder 'I6' was an interior girder with a nominal 6-ft wide deck. Girder 'X4' was an exterior girder with approximately 4 ft of curb and deck remaining. Note that the dimensions for the slab width shown in Figure 2 are nominal dimensions and that the actual dimensions varied slightly along the length of the test girders.

In general the girders performed well in load tests even after 50 plus years of service. In spite of having thin webs and minimal shear reinforcement each of the girders had experimental capacity greater than the code calculated nominal shear capacity. Results indicate that the girders supported load through a tied-arch mechanism wherein the concrete carried compressive loads as an arch, and the prestressing strand acted as ties. The effects of the slab width on shear capacity where not evident from the limited data. The results do demonstrate, however, that the curb increased the strength and stiffness of the exterior girders relative to the interior girders.

A brief discussion of truss and tied-arch mechanisms in concrete beams is presented in the literature review contained in Appendix A. Readers unfamiliar with these concepts may benefit from reviewing this material prior reading the results section of this appendix.

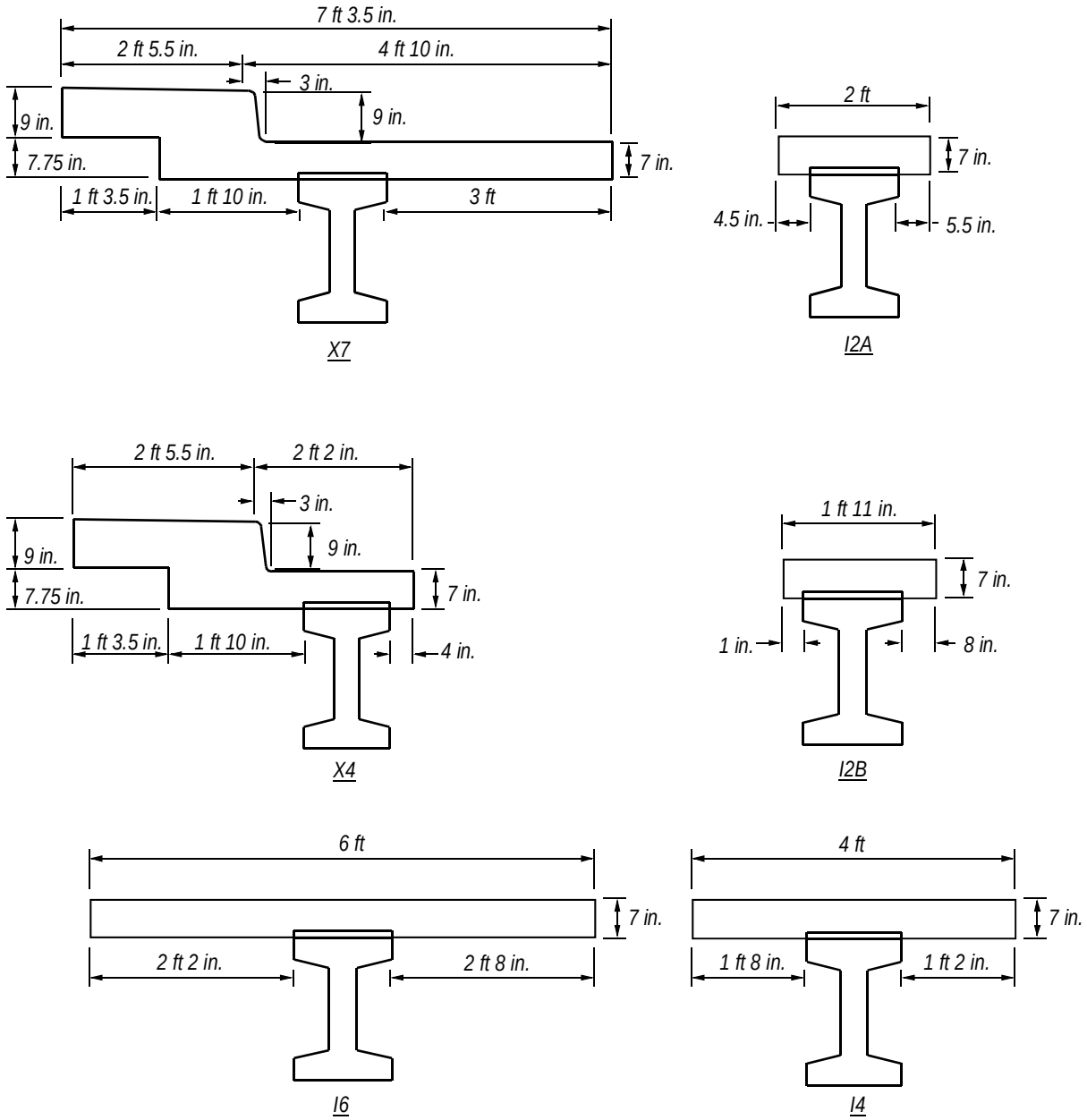

Figure 2–Test girder identifications and slab configurations

2 Girder and Deck Design

Test girders were salvaged from a bridge on Florida Highway SR-72, in Sarasota County, Florida. Girders were precast and pretensioned, having the cross section shown in Figure 3.

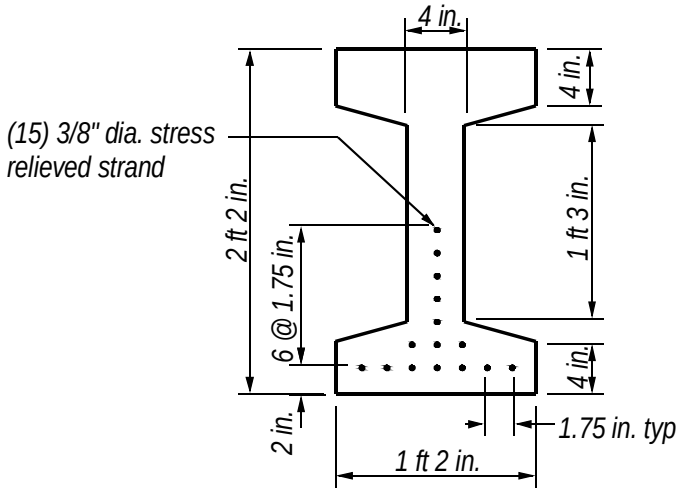

Figure 3–Typical girder cross section

Construction drawings dated February 1954 are shown in Appendix H. These drawings specified that each girder be prestressed with (15) 3/8-in. diameter stress-relieved strands pretensioned to 14 kip each. The strand pattern is shown in Figure 3. No records from pretensioning operations are available, however the effective prestress force of girder I2A was experimentally evaluated using the method presented Pessiki et al. (1996).

The specified 28-day compressive strength was 5500 psi for the girders and 3600 psi for the deck. Core samples from the girders were taken and tested in 2006. Results of the core tests are presented in Appendix H and indicate that the average concrete compressive strength was 3240psi.

Construction drawings specified two #4 longitudinal bars in the top flange and (12) #4 vertical bars spaced at 6 in. o.c. at each end of the girders (Figure 4). The vertical bars did not have hooks specified. End blocks extended 2.5 ft from each end. Non-destructive testing was used to locate the vertical bars in the web. Results of non-destructive testing are presented in section 4.1.

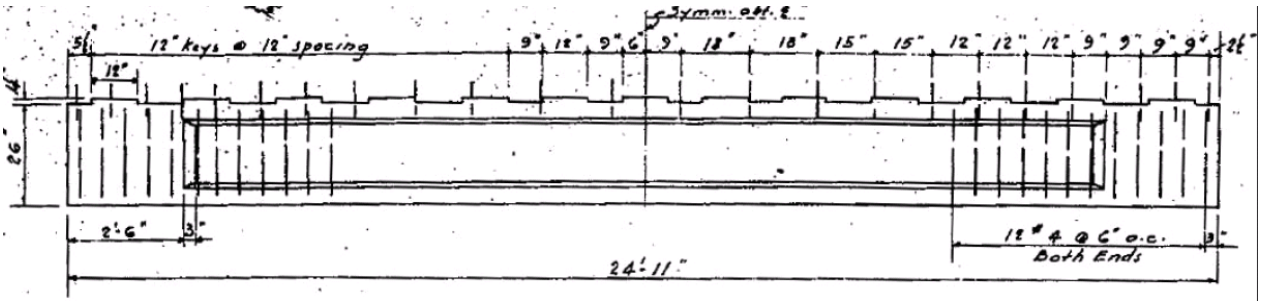

Figure 4–Transverse reinforcement

The girder plans called for shear keys (Figure 4) on top of the girders to create composite action with the cast-in-place deck. Hoops were specified to tie the girders and deck. The hoops were #4 bars and were partially embedded into the top flange, with the remaining portion extending above the girder and embedded into the deck. Plans specified (24) hoops total for each girder, with 9 in. spacing at the ends, and 18 in. spacing near mid-span.

Figure 5 shows the curb and deck reinforcement specified on the original plans. Original plans are included in Appendix H. Plans called for a 7-in. thick cast-in-place deck reinforced with longitudinal and transverse #4 bars top and bottom. Longitudinal bars were specified at an average of 12 in. oc in the bottom of the deck, and 18 in. oc in the top. Specified transverse reinforcement was #4 bars at 10 in. oc in the top and bottom of the deck. Additional transverse #4 bars were spaced at 10 in. oc and were bent such that they support negative moments over the girders and positive moment between girders. Curb reinforcement was (3) #4 bars placed longitudinally near the top of the curb, and bent #4 bars spaced at 12 in. oc transversely to tie the curb to the deck.

End diaphragms were cast between the girders and each end of the bridge and had a specified thickness of 8 in. with 1-in. diameter threaded bar extending through the end diaphragms and girder end blocks to tie the bridge together transversely. Varying portions of the end diaphragms were retained with individual test girders. Relevant details about the end diagrams are given in the next section.

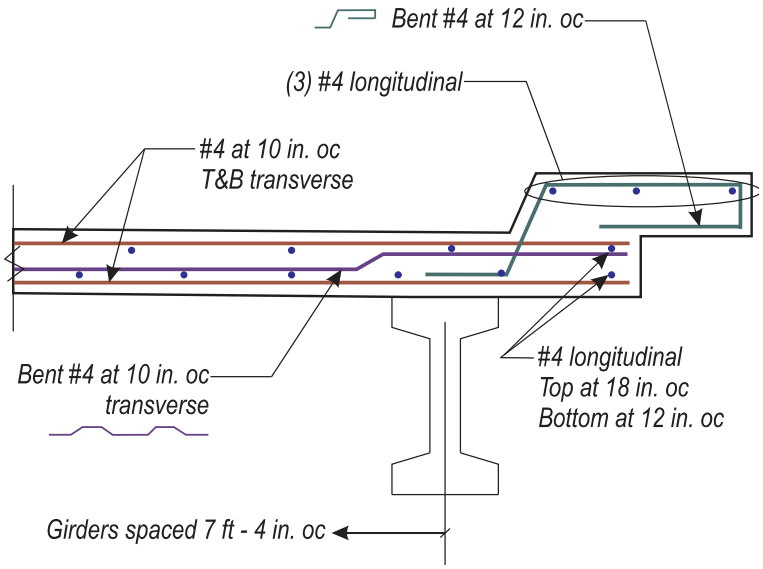

Figure 5–Deck and curb reinforcement

3 Test Setup, Procedures, and Instrumentation

Girders were tested in three-point bending. Dimensions and setup are described in Figure 6 and Table 1. The support nearest the load point is referred to as the near support. The opposite support is referred to as the far support.

The load was transferred from a hydraulic actuator to the girders through a 10-in. x 10-in. x 2-in. thick reinforced neoprene bearing pad at a loading rate of approximately 0.25 kip/second. A load cell was used to measure the applied load. A thin grout pad (1 in. maximum thickness) was placed below the load point on X7, 12B, X4 and I4 to compensate for slight cross-slopes of the deck on those girders.

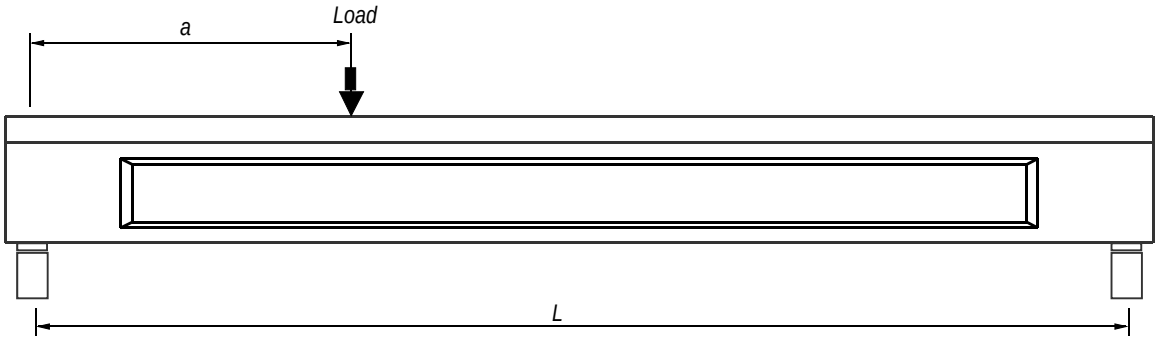

Figure 6–Test setup

Table 1–Test setup dimensions

Girder	A	a/d*	L
X7	8’-2”	3.4	23’-9”
X4	8’-2”	3.4	24’-3”
I2A	10’-11”	4.5	23’-9”
I2B	8’-1”	3.3	24’-11”
I4	5’-2”	2.1	23’-10”
I6	8’-2”	3.4	24’-0”
*d = 29 in.			

Linear Variable Displacement Transducers, LVDTs, were used to measure vertical displacements at the load point and above each support. LVDTs were also used to measure strand slip. A steel frame was bolted to the end of each beam to support the strand slip LVDTs (Figure 7). In total, ten strands were monitored for slip (Figure 8). LVDTs were also used to measure lateral movement at the load point of girders X7 and X4.

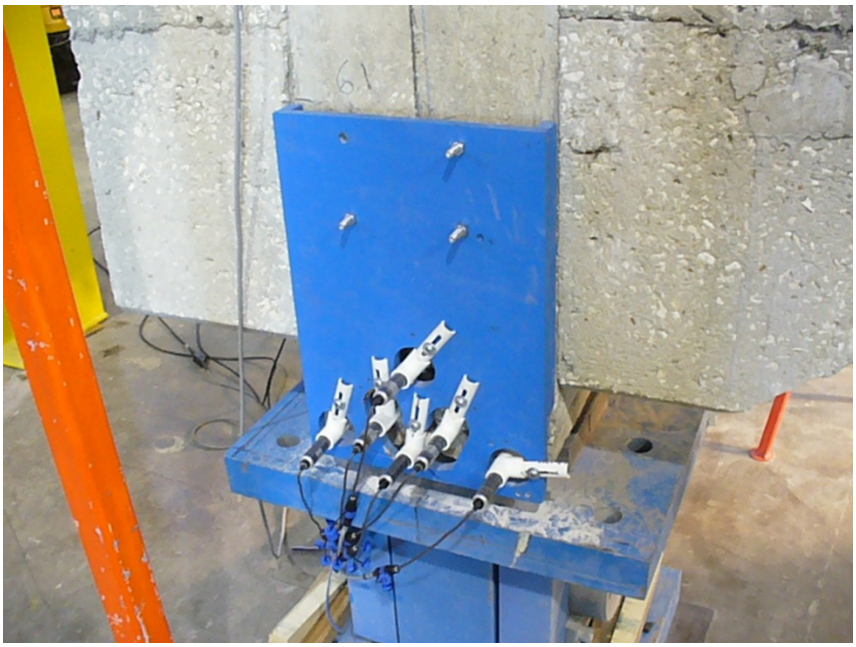

Figure 7–LVDTs at end of girder

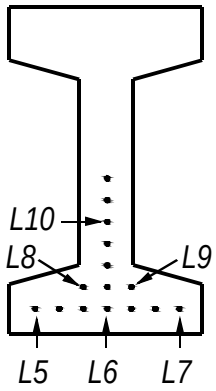

Figure 8–Strands instrumented with LVDTs

Typically, girders were supported at each end on an 8-in. x 14-in. x 2-in. thick (14-in. dimension perpendicular to the length of the girder) reinforced elastomeric bearing pad. Additional bearing points were added at the far support of girders X7, X4 and I6 to provide stability during testing. The additional bearing pads were placed below the end diaphragm or curb as shown in Figure 9, Figure 10, and Figure 11.

Figure 9–X7 far support

Figure 10–X4 far support

Figure 11–I6 far support

Bonded foil strain gages were used to measure concrete surface strain and to detect cracks during testing. Strain gages had a 60-mm gage length. Appendix H contains information on the labels and locations of all strain gages and LVDTs used during load tests.

4 Results and Discussion

Results of the load tests are presented in terms of superimposed shear. Superimposed shear is defined as the shear force at the near support due to the load applied by the hydraulic actuator. The superimposed shear does not include shear force due to girder self-weight.

Displacement results presented in this section are vertical displacement at the load point. Vertical deflection at the load point was taken as the average displacement recorded by the LVDTs on either side of the load point, less the displacement of the girders due to bearing pad compressive reactions. In some cases, the two LVDTs at the load point reported different displacements, indicating that the girder was rotating in addition moving vertically. Rotation of the girders is discussed with the results from in the individual load tests.

Strand slip was monitored using LVDTs mounted on the back of the girders above the near support. Data from the LVDTs indicated that strand slip only occurred during testing of X4. Because strands did not slip in the other tests, slip data is only presented for test X4.

4.1 Non-destructive testing to locate transverse reinforcement

Transverse reinforcement in the webs was located using a cover meter. Girder construction drawings specified that (12) #4 single-leg transverse bars be placed vertically at 6 in. o.c. at each end (Figure 4). Of the (12) bars, (6) of the bars were to be placed in the end block and the other (6) placed in the web. The location of the transverse reinforcement in the end blocks could not be determined because the clear cover over the reinforcement was too large for the cover meter to penetrate.

To avoid interference from the prestressing strands, only the top of the web was scanned with the cover meter. Thus, the spacing and quantity of the vertical reinforcement were determined, but the orientation (inclination) of the bars could not be determined. Figures showing the transverse steel locations as determined by the cover meter are presented with the results of the individual girder tests. Note that the presumed vertical orientation of the reinforcement shown in the figures was not confirmed.

Transverse reinforcement in the test girders was generally not consistent with the construction drawings. For example, only two of the twelve ends had the specified number of transverse bars in the web. Four of the twelve ends had only two vertical bars in the web. Inconsistency between the specified and observed vertical reinforce is particularly troubling

because the specified reinforcement was already minimal compared to modern girders. It is recommended that similar girders in Florida be analyzed under the assumption that vertical reinforcement is absent. Alternatively, it is recommended that a cover meter or other means be used to locate vertical reinforcement for the analysis.

4.2 Test X7

Girder X7 was load tested at an a/d ratio of 3.4. Shear-displacement behavior of X7 is shown in Figure 12. As load was applied the girder displaced vertically and latterly, and rotated about its longitudinal axis. Lateral displacement is presented in Figure 13. The maximum rotation was approximately 0.14 degrees, as determined from LVDTs L2 and L3 which were placed on either side of the load point. The rotation and lateral movement are attribute in-part to the asymmetric cross-section and load location which was not through the section's shear-center. Uneven bearing pad deformation may also have contributed to the rotation. As previously discussed, and as presented in Figure 9, multiple bearing points were placed at the far end of X7 to prevent instabilities due to asymmetry of the cross-section and load.

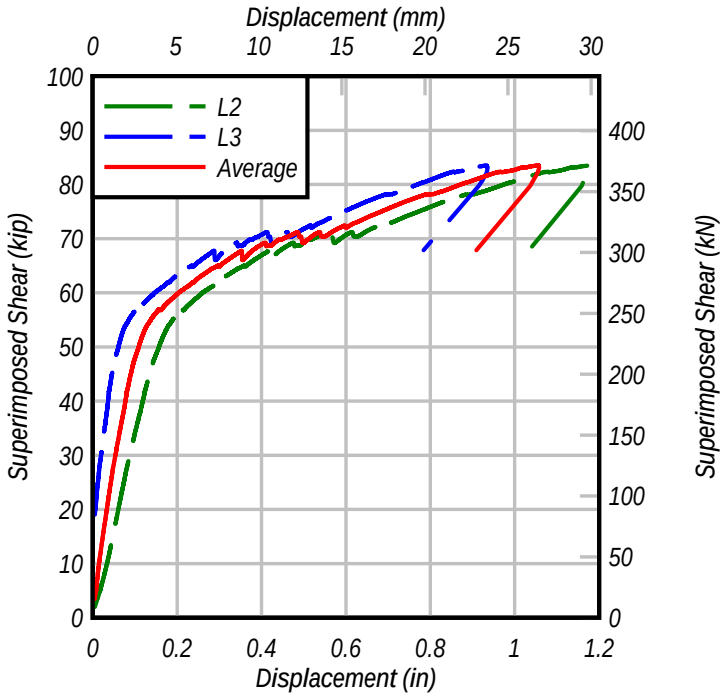

Figure 12–X7 shear vs. vertical displacement

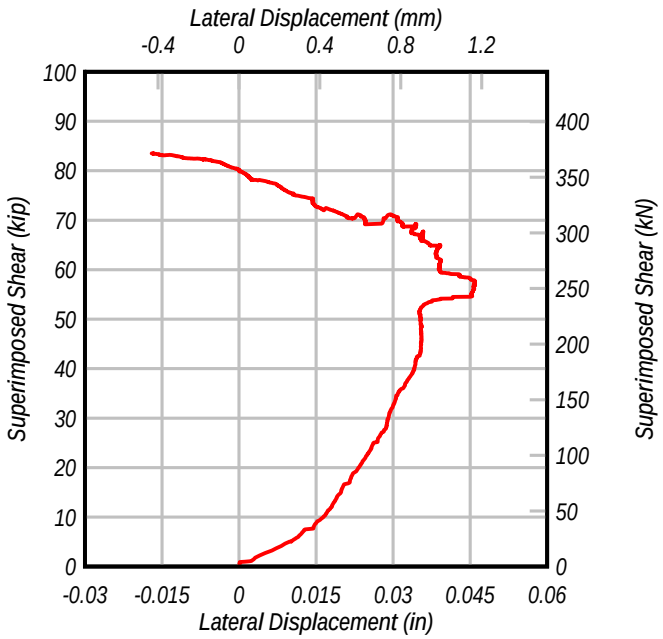

Figure 13–X7 lateral displacement at load point

The girder behaved linear-elastically until the formation of cracks. Visible cracking was first observed in the web at a superimposed shear load of approximately 51kip (Figure 14). Although cracks were not visible prior to 51kip, data from rosette R7 indicates that the crack first formed at a shear of 41kip (Figure 15). At 58kip of shear, the initial crack in the web was observed to have joined with a flexural crack in the bottom flange. This load corresponds to the change in slope on the shear-displacement plot; the change in stiffness being attributed to cracking.

Referring to Figure 12, the abrupt changes in the shear-displacement curve between 65kip and 70kip correspond to the formation of additional cracks. Cracks formed farther from the load point and at shallower angles as the load increased. Comparing the final crack pattern with the location the transverse reinforcement (Figure 14), it is noted that with only one exception, the cracks did not cross transverse reinforcement. Thus, after cracking the load could not have transferred through truss action, but rather was carried through arch action. Girder X7 supported a maximum superimposed shear of 84kip. At this load a punching shear failure occurred in the slab and curb. Figure 16 is a photo of the curb side of X7 showing the location of the punching failure. The red strap in the picture is from the crane which was lifting the girder as the photo was taken.

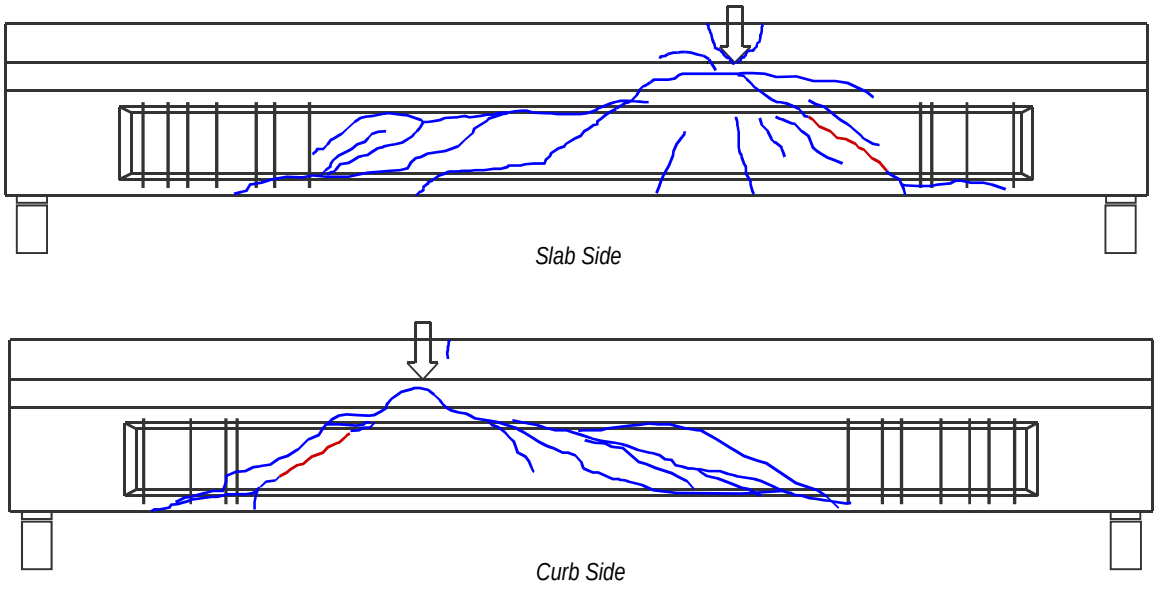

Figure 14–X7 cracks (initial crack in red)

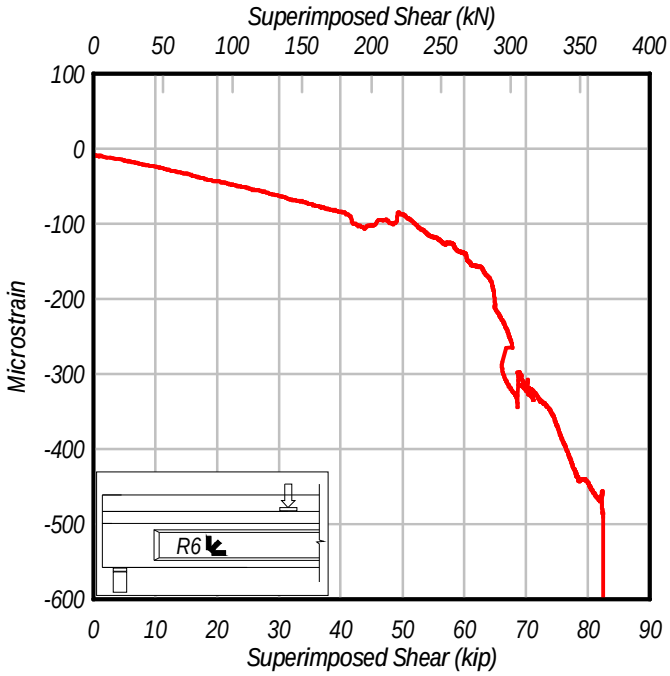

Figure 15–X7 rosette R7

Figure 16–X7 punching failure bottom view

Strain gages were placed around the cross-section at three sections along the length of the girder. Data from theses gages were combined via linear interpolation to approximate the strain contour of the section during loading. Figure 17 shows the strain contour at the section below the load point at a shear of 45 kip. The maximum compressive strain occurred at the top corner of the curb. Because the section experienced biaxial bending, the strain contours were inclined.

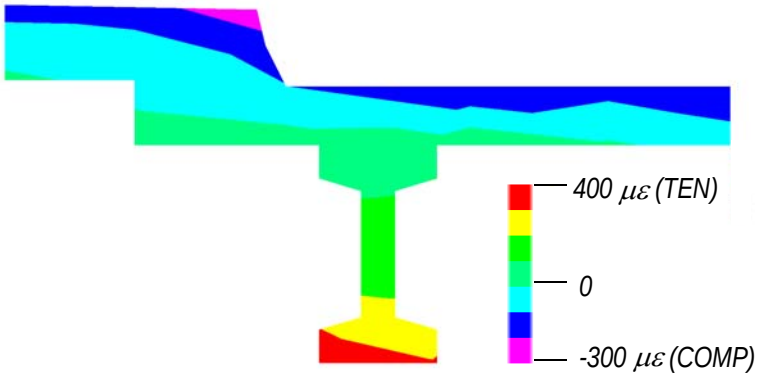

Figure 17–X7 Strain contour at shear of 45 kip at section below load point

4.3 Test X4

Girder X4 was loaded at an a/d ratio of 3.4. During load testing X4 displaced vertically (Figure 18) and laterally (Figure 19), and rotated about its longitudinal axis. The maximum rotation was approximately 0.11 degrees as determined from the differential displacement reported by LVDTs placed on either side of the load point. Rotation and lateral movement are

attributed to the asymmetric cross-section and load location which was not through the shear-center of the section. Uneven bearing pad deformation may also have contributed to the rotation. As previously discussed, and as presented in Figure 10, multiple bearing pads supported X4 at the far end to prevent instabilities due to asymmetry of the cross-section and load.

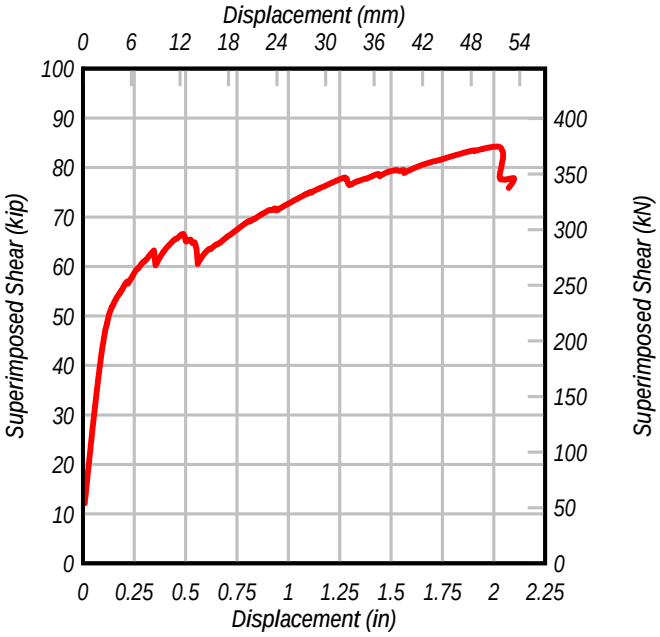

Figure 18–X4 shear vs. displacement

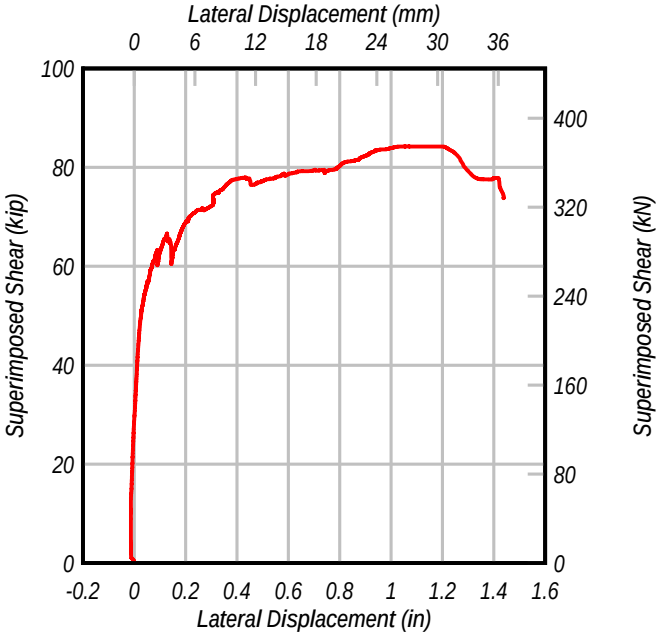

Figure 19–X4 lateral displacement

Referring to Figure 18, girder X4 behaved linear-elastically until a superimposed shear of about 45kip. The transition from linear-elastic behavior corresponded to the formation of flexural cracks at the bottom of the girder below the load point (Figure 20). Data from gage S25 (Figure 21) indicate that cracking initiated at a shear of 44kip. Initial cracks were first visually observed at a shear of 56kip.

The abrupt changes in the shear-displacement plot at 62kip and 66kip correspond to the formation of incline cracks in the web. Cracks continued to form farther from the load point and at shallower angles as the load increased. At the final stages of the load test incline cracks had a maximum width of 1 in. As shown in Figure 20 vertical reinforcement was not engaged by the inclined cracks. The relatively large crack widths and absence of engaged vertical reinforcement suggest that the girder supported load by arch-action.

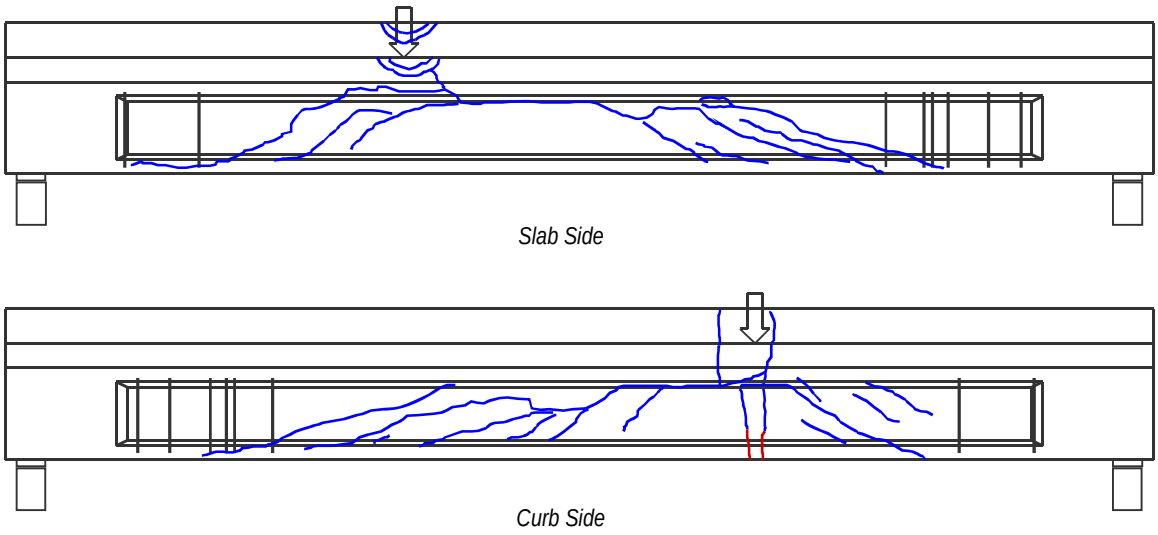

Figure 20–X4 cracks (initial cracks in red)

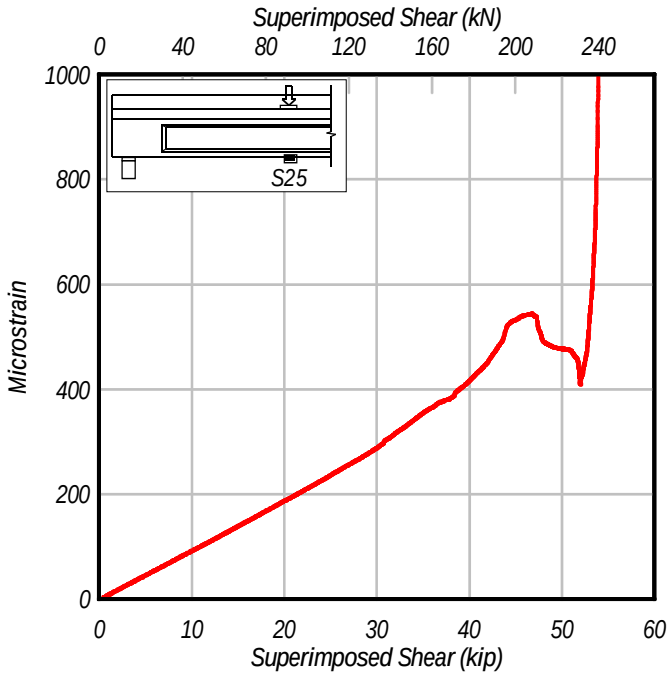

Figure 21–X4 shear vs. strain S25

Strain gages were placed around the cross section to evaluate the flexural strain field during load testing. Figure 22 shows the strain field at the section below the load point at a superimposed shear load of 46k. Contours indicate biaxial bending with the neutral axis inclined at approximately 20 degrees from horizontal. The largest compressive strains occurred in the upper corner of the curb and slab. Formation of the initial flexural cracks on the curb side is consistent with the measured strain field which recorded the largest tensile strains at the location of cracking.

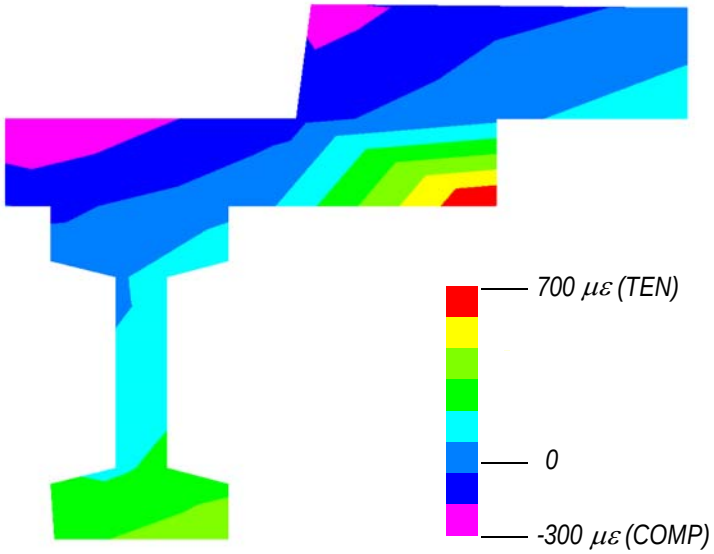

Figure 22–X4 strain field at load location at a superimposed shear of 46 kip

Lateral displacement of girder X4 is presented in Figure 19. As with vertical stiffness, the lateral stiffness of the girder was reduced by the formation of cracks. The relatively flat portion of the shear-displacement curves at the latter stages of the test suggests that reinforcement may have yielded.

Crushing of the compression zone in the slab near gage S15 began at a shear of 71kip. Examining data from S15, the compressive strain reached 2200 microstrain prior to crushing (Figure 23). Crushing is attributed to the superposition of bearing strain from the load point and the flexural strain. The corner of the slab near S15 continued to crush and spall as the shear increased beyond 71kip. The corner of the curb near gage S17 began to crush at a shear of 76 kip. According to gage S17, the strain at the corner of the curb reached 2550 microstrain immediately prior to crushing (Figure 23). Girder X4 supported additional load after the initial crushing at the corners of the slab and curb, reaching a maximum superimposed shear of 84kip. As previously noted, the girder behaved as a tied-arch in the final stages of loading. The failure mode of Girder X4 was flexural compression failure of the concrete. The moment at failure was 95% of the calculated nominal moment capacity. Details of nominal capacity calculations are presented in a later section.

Girder X4 was the only test in which the strands exhibited significant slip (Figure 24). The strand monitored by LVDT L7 was located the curb side in the bottom row. This strand was in the region of highest tension in the bottom flange (Figure 22). Slipping of the strands in X4

contributed to the rotation about the load point and crushing of the compression zone. Because X4 failed in flexural the strands in this girder likely supported higher loads than in other girders, making slip more likely. Slip was also augmented by the asymmetric bending as demonstrated by the slip L7.

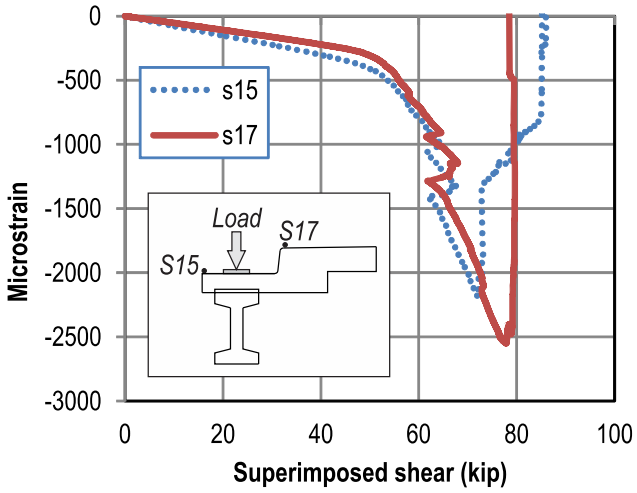

Figure 23–X4 shear vs. compressive strain

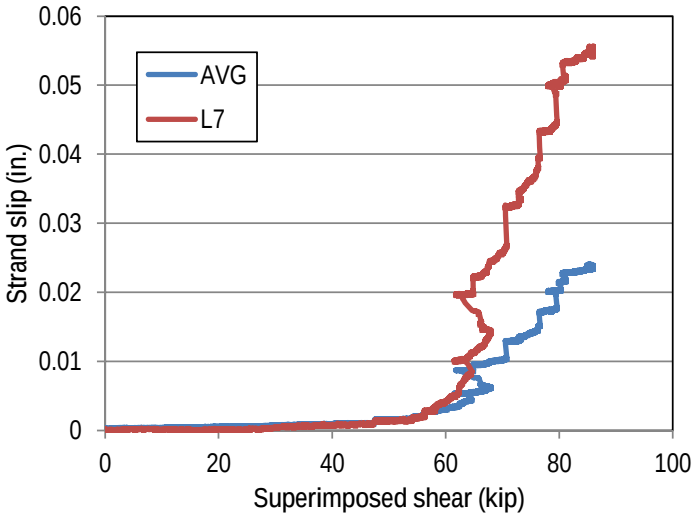

Figure 24–X4 strand slip vs. shear

4.4 I2A-Determination of Effective Prestress

The effective prestress force of Girder I2A was determined using to the procedure presented by Pessiki et al. (1996). Based on this procedure, girder I2A was loaded until flexural cracks formed. Two flexural cracks were visually observed at a superimposed shear reached 36k (Figure 28). The load was held constant at this force so that the cracks could be marked. After cracks were marked the girder was unloaded and strain gages (oriented longitudinally) were placed as close as possible to, and on each side of both cracks (Figure 25).

Girder I2A was loaded to failure after the initial cracks were marked and strain gages were installed. Figure 26 shows applied load vs. strain data from each strain gage placed adjacent to the flexural cracks. Theoretically, as load is increased, the cracks should open when the tension the tension due to bending equals the precompression from the effective prestress force. This behavior is indicated by a bilinear shape in the load-strain plots shown in Figure 26. At a load of 40kip (22kip shear) the load-strain relationship became nonlinear due to reopening of the flexural cracks. Knowing this load at which the cracks reopened (i.e. precompression force was overcome), the effective prestress force in the girder was calculated using flexural theory. Specified initial prestress force, effective prestress force and total losses are shown in Table 2. Note that calculation of the experimental prestress force utilized flexural stiffness properties derived from the experimental load-displacement data.

An effective prestress force of 112kips was calculated from the experimental data. Assuming an initial prestress force of 210kip as per the construction drawings, the experimental data indicate a 47% loss in prestress force. This value of prestress loss is unusually high suggesting that the initial prestress force may have been less than specified. This would not be unreasonable considering other inconsistencies between the girders and plans, such as placement of vertical reinforcement. It is not known if the experimentally evaluated prestress force from I2A was representative of all test girders.

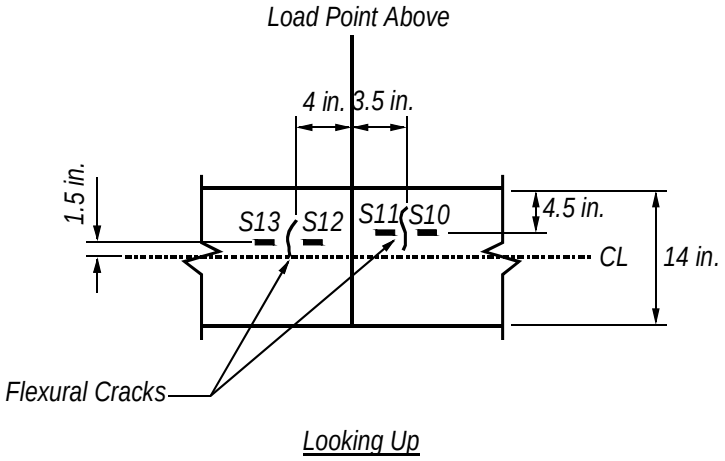

Figure 25–I2A decompression gages

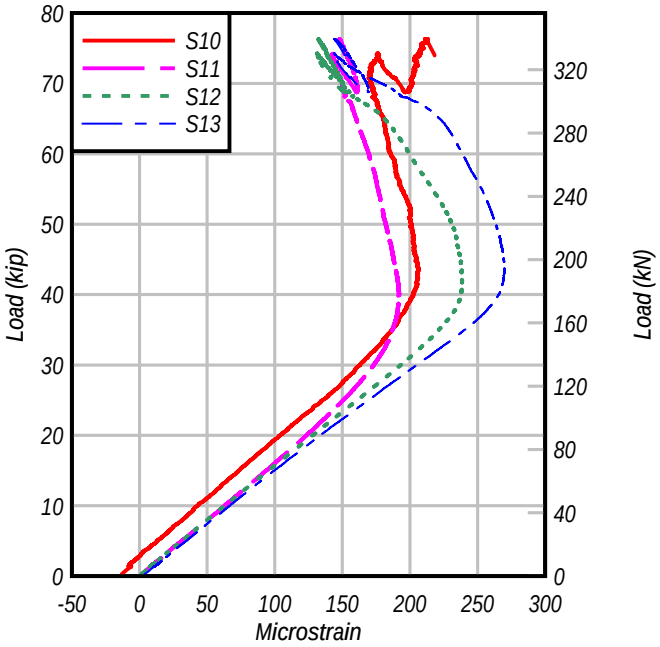

Figure 26–I2A load vs. decompression strain (crack opening)

Table 2–I2A specified and effective prestress force

Specified Initial Prestress Force	Experimental Effective Prestress Force	Total Losses
210 kips	112 kips	47%

4.5 Test I2A

After evaluating I2A for effective prestress, the specimen was loaded to ultimate load. Load was applied at an a/d ratio of 4.5. Shear-displacement data from the ultimate load test is presented in Figure 27. Contrary to X4 and X7, girder I2A did not rotate about its long axis during loading. Flexural cracks reopened at a load 40 kip, corresponding to 22 kip superimposed shear. According to the shear-displacement plot, significant deviation from linear-elastic behavior did not occur until the shear reached 36k. Softening of the girder corresponded to the propagation of flexural cracks. The abrupt changes in the shear-displaced data at shear forces near 40 kip were due to the formation of inclined cracks in the web. As the load increased, additional cracks formed farther from the load point and at shallower angles. Cracking in the web between the load point and the near support was particularly severe, as noted by the shaded area in Figure 28 and shown in Figure 29.

Cracks along the web-flange interface in the shear span prevented the transverse reinforcement from developing and carrying forces. On the far support side of the load, the cracks did not engage the transverse reinforcement. Incline cracks on both ends of the beam were too wide to allow force transfer by aggregate interlock. Without aggregate interlock and effective transverse reinforcement, the girder behaved as a tied-arch during the final stages of loading.

Failure was precipitated by the formation of tensile cracks in the top of the arch between the near support and load point. After the cracks formed, the arch became unstable, buckled upward (Figure 29) and lost load carrying capacity. Failure occurred at a superimposed shear of 51 kip. This behavior was captured by gage S1 (Figure 31) located on top of the girder. After inclined cracks formed in the web, the compressive strains on top of the slab at gage S1 decreased suddenly. As testing continued strain reported by S1 became tensile. This tensile action at the top of I2A resulted in cracking and instability of the compression load path. This type of failure has also been reported by Kostovos (1987).

Girder I2A was one of two tests (I4 being the other) in which cracks formed in the end block. LVDT data indicate that the end block cracks did not affect strand slip.

Extensive cracking and spalling in the web exposed the transverse reinforcement (Figure 29). Orientation and spacing of the transverse bars were not consistent with the girder plans.

Rather than being oriented vertically, bars were inclined towards the load point. Also, the bars were spaced much closer than the specified 6” o.c. spacing.

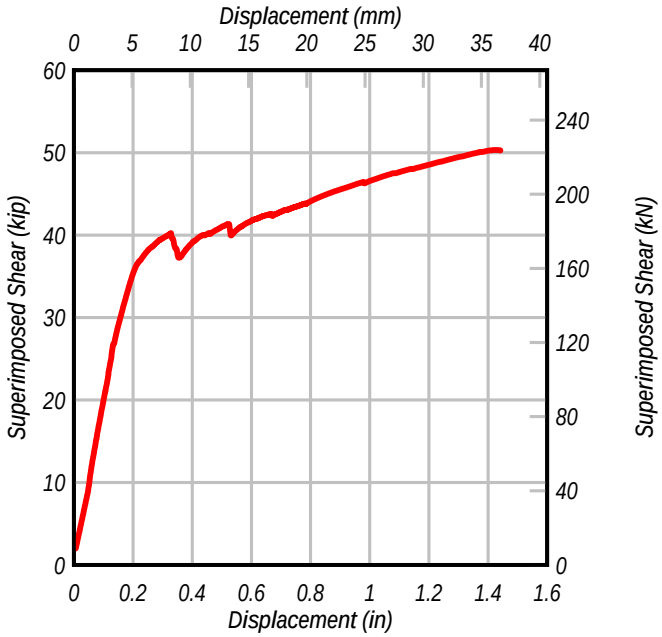

Figure 27–I2A shear vs. displacement

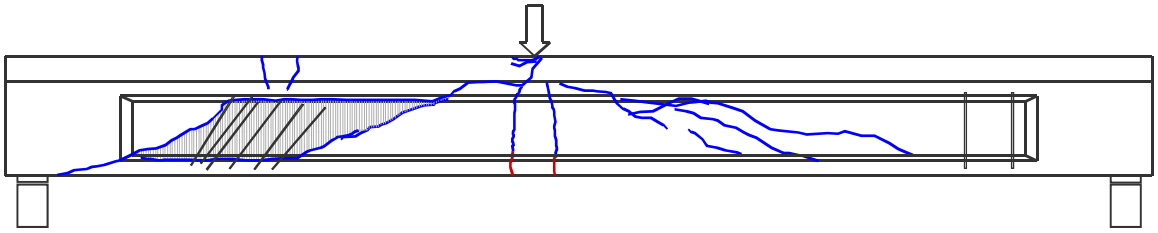

Figure 28–I2A cracks (initial cracks in red)

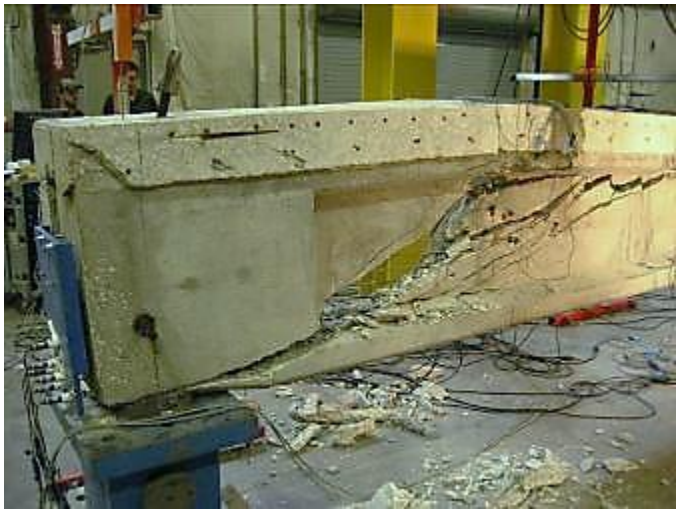

Figure 29–I2A incline cracks in web

Figure 30–I2A transverse reinforcement-arch failure

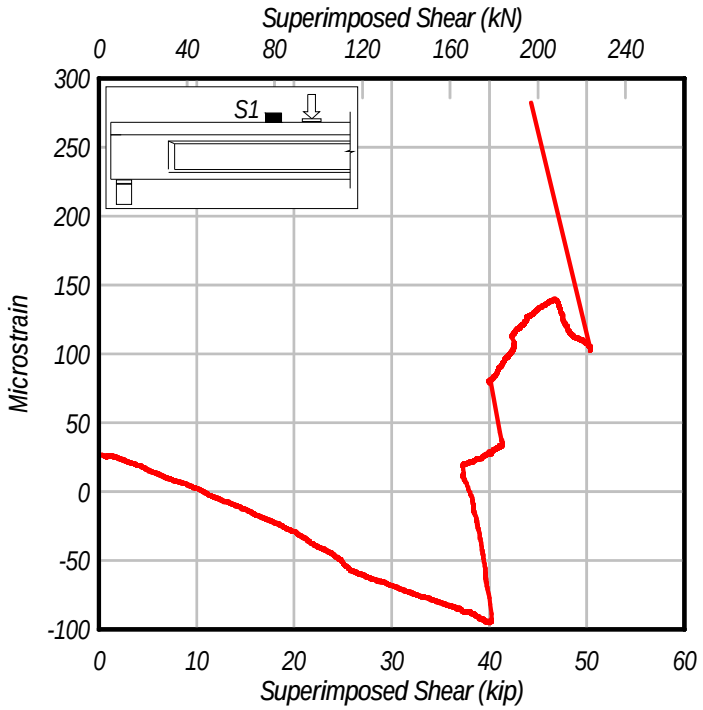

Figure 31–I2A shear vs. strain S1

4.6 Test I2B

Girder I2B was loaded at an a/d ratio of 3.3. Figure 32 shows the superimposed shear vs. load point displacement. I2B rotated 0.22 degrees about its long axis as the shear increased from 0kip to 5kip. The girder maintained this rotated orientation for the remainder of the test. Girder I2B behaved linear-elastically until the shear reached about 43kip, at which point flexural cracks formed below the load point (Figure 33). After formation of the initial cracks, load was held constant and the cracks were marked. After loading was resumed, inclined cracks formed in the web and additional flexural cracks formed in the bottom flange. Loading was stopped again to mark the cracks at 50kip of shear. The abrupt change in the shear-deflection plot at 50kip was due to relaxation of the load while cracks were being marked. Loading was again resumed, and additional shallower cracks formed farther from the load point towards the far support. One of these cracks formed at the peak load of 67kip. The load supported by the girder dropped after the formation of the crack at 67kip, and the load was held to mark cracks for the final time. After loading resumed, the inclined cracks near the far support continued to open and propagate,

however the girder was unable to support the previous peak load. The test was terminated when the load dropped to 64kip.

Comparing the locations of cracks and transverse reinforcement (Figure 33), it can be seen that cracks between the load and near support intersected transverse bars whereas cracks towards the far support did not. As the cracks towards the far support were large, it is unlikely that shear was carried by aggregate interlock at that end of the beam. Thus it is believed that the near side of the girder supported load by some combination of arch and truss action, and the far side supported load by arch action.

The limiting factor on ultimate strength of I2B was capacity of the web near the far support to withstand the formation and propagation of inclined cracks. Additional displacement beyond peak displacement would have resulted in failure of the truss and/or arch mechanisms; however it is unlikely that additional displacement would have accompanied load in excess of the previous peak. It is concluded that the girder strength was controlled by the web capacity, and it is presumed that the displacement capacity would have been controlled by failure of the arching action.

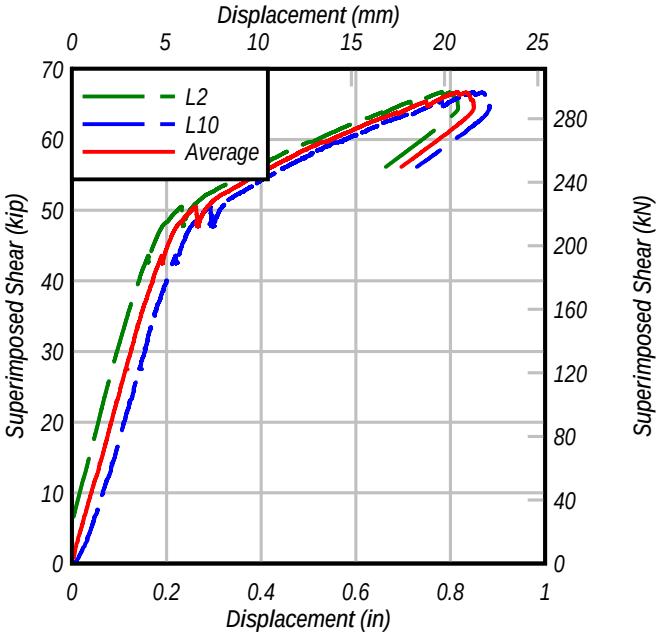

Figure 32–I2B superimposed shear vs. displacement

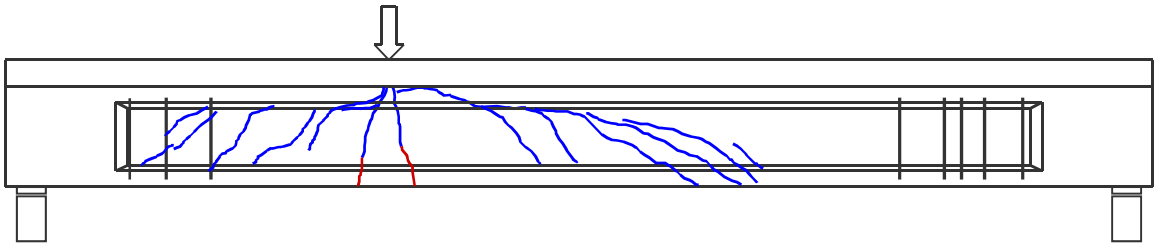

Figure 33–I2B crack pattern (initial cracks in red)

4.7 Test I4

Girder I4 was loaded at an a/d ratio of 2.1. Figure 34 shows the superimposed shear vs. load point displacement. I4 began rotating about its long axis as soon as load was applied. The angle of rotation increased with increasing load, reaching a maximum of 0.57 degrees just before failure.

The first crack formed at a shear of 38 kip as reported by rosette R2 on the web (Figure 35). The initial crack was an incline crack in the web (Figure 36), and appears to have had little effect on the girder stiffness as measured by the shear-displacement relationship. Stiffness of the girder changed at a shear of 75 kip. This is the same load at which the inclined crack near gage R2 was first visually observed.

As the load was increased additional cracks formed in the web on the far support side. The cracks formed farther from the load point and at shallower angles at higher loads. The abrupt changes in the shear-displacement plot near 112 kip and 118 kip correspond with formation of inclined cracks towards the far support. During the final stages of loading cracks in the web were wide approximately 0.5in wide. As shear could not transfer across the cracks, and as the cracks did not engage transverse reinforcement, it is believed that the end of the girder towards the far support behaved as a tied arch during the final stages of loading. The peak superimposed shear supported by girder I4 was 118k.

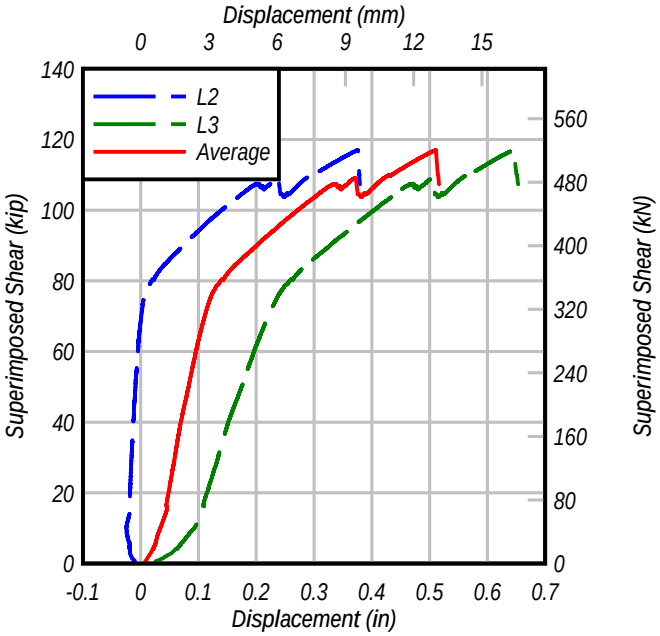

Figure 34–I4 shear vs. displacement

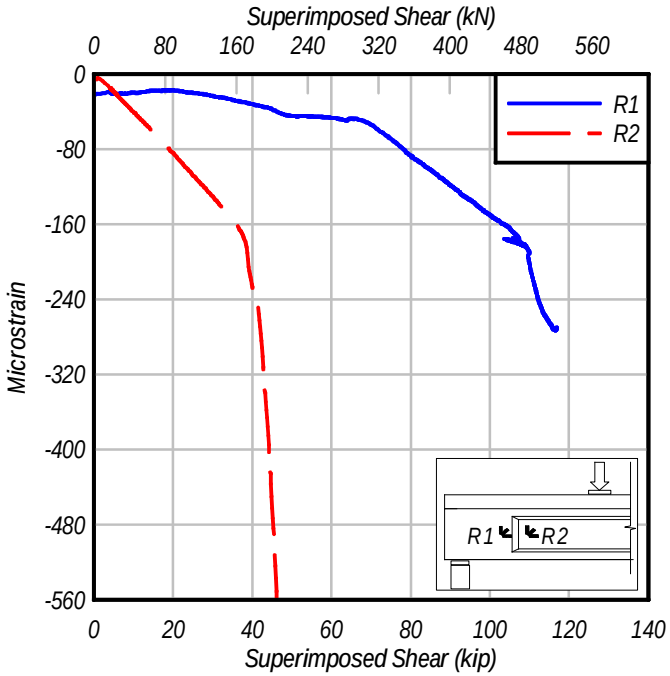

Figure 35–I4 principal strain vs. shear

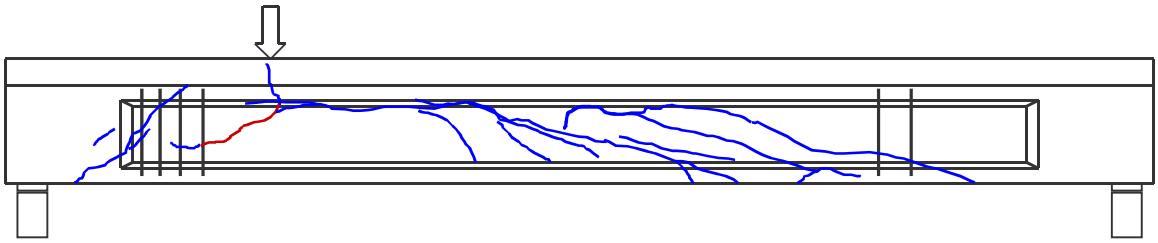

Figure 36–I4 cracks (initial crack in red)

Cracks towards the near support engaged transverse reinforcement (Figure 36). The transverse reinforcement slowed the propagation and opening of these cracks as compared to cracks at the far end of the girder. The shear load transferred to the near support is believed to have been carried by truss action. The shear transfer towards the far support was likely carried by arch action.

The limiting factor on girder strength was capacity of the web on the far support side to withstand the formation and propagation of inclined cracks. Additional movement beyond peak displacement would have resulted in failure of the truss and/or arch mechanisms, however it is unlikely the addition displacement would have resulted in that the loads in greater than the observed peak. It is concluded that the girder strength was controlled by the web capacity and that the displacement capacity was controlled by the arching and/or truss action.

Although cracks formed in the end block, no strand slip was reported by the LVDTs.

4.8 Test I6

Girder I6 was loaded at an a/d ratio of 3.5. Figure 37 shows the superimposed-shear versus load-point displacement. The girder behaved linear elastically until the first crack formed at a shear of 43kip. Load at cracking was determined by data from gage S29 (Figure 38). The initial crack was a flexural crack below the load point (Figure 39). Inclined cracks formed in the web toward the near support at a shear of 48kip. Shallower cracks formed farther from the load point as the load was increased. The load test was terminated after a sudden drop in load caused by the formation of an incline crack at the far end of the girder. The maximum superimposed shear was 68kip. Girder I6 did not rotate as load was applied.

Comparing the cracks with the locations of transverse steel (Figure 36), cracks intersected transverse reinforced on the near side of the beam, but not on the far end. Shear was carried by truss action to the near support, and arch action to the far support.

The limiting factor on girder strength was capacity of the web on the far support side to withstand the formation and propagation of inclined cracks. Additional displacement beyond the tested peak would likely have resulted in failure of the truss and/or arch mechanisms, however it is unlikely the additional displacement would have resulted in that the loads in excess of the observed peak. Girder strength was controlled by the web capacity and it is presumed that displacement capacity would have been controlled by failure of the arch and/or truss mechanisms.

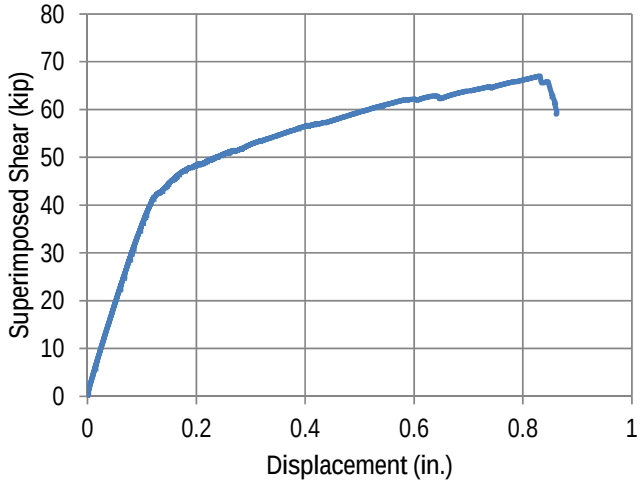

Figure 37–I6 shear vs. displacement.

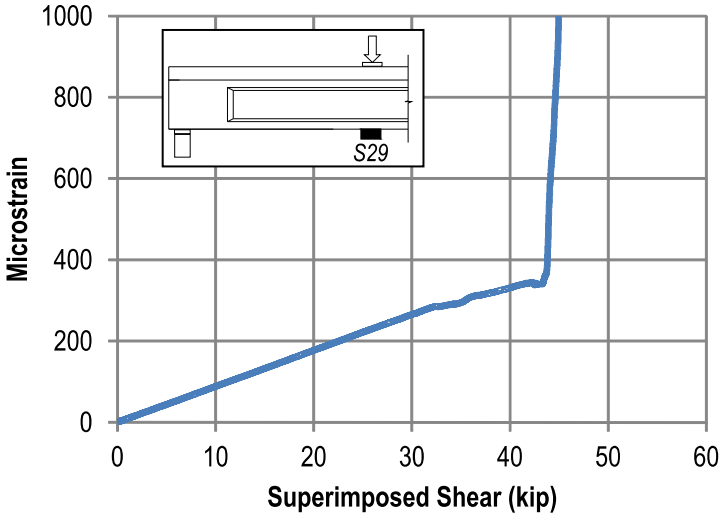

Figure 38–I6 gage S29 vs. shear.

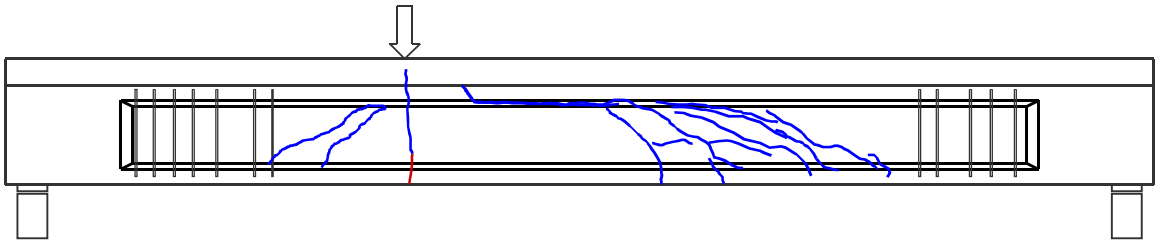

Figure 39–I6 cracks (initial crack in red).

5 Comparison with computed strength

Experimental ultimate capacity was compared with the nominal shear and moment strength calculated using the detailed procedure from ACI 318 (ACI 2008) and the general (MCFT based) procedure from AASHTO LRFD (AASHTO 2007). Nominal shear capacities were calculated for an interior girder using the specified reinforcement, prestressing, geometric properties, and material properties. This approach was used because physical properties were not tested for each girder and because this is the likely approach of an engineer performing a load rating on the bridge.

Based on the girders for which concrete compressive strength and effect prestress were tested, it is assumed that the specified properties are unconservative relative to the physical properties. Thus the approach used for shear calculations resulted in nominal capacities larger than the capacities calculated using the available tested properties. This effect of the approach is inconsequential considering that the experimental capacities were significantly higher than the nominal capacities as shown in Figure 40 and Table 3.

Figure 40 shows the code calculated nominal capacities plotted against the shear span length (a). The discontinuity at $a = 5.7$ occurs due to the specified termination of transverse reinforcement at that location. Point data on the figure represent the experiment shear capacity of the test girders. The experimental capacity of the girders was taken as the maximum superimposed shear plus the dead load shear. In each case, the experimental capacities of the girders were greater than the theoretical capacities predicted by ACI and AASHTO codes. Also note that the exterior girders exhibited 30% greater shear capacity than the interior girders tested at the same shear span.

Data from Figure 40 are tabulated in Table 3. The average experimental shear capacities were 1.96 and 2.10 times larger than the capacity of the standard girder predicted by ACI and AASHTO, respectively. The average experimental-to-nominal capacity ratio for the exterior girders was 2.56 (ACI) and 2.71 (AASHTO), compared to 1.66 (ACI) and 1.79 (AASHTO) for the interior girders. This increased capacity of the exterior girders is attributed to the shear capacity of the curb. As the test girders tended to behave as tied-arches prior to failure, the presence of the curb contributed to the strength of the arch and thus to the shear capacity of the girder.

The increase in nominal shear strength of the test specimens due to the curb can be conservatively approximated by multiplying the shear nominal capacity of an interior girder by the ratio of the exterior girder depth to interior girder depth. This is demonstrated by the calculations shown in Table 5.

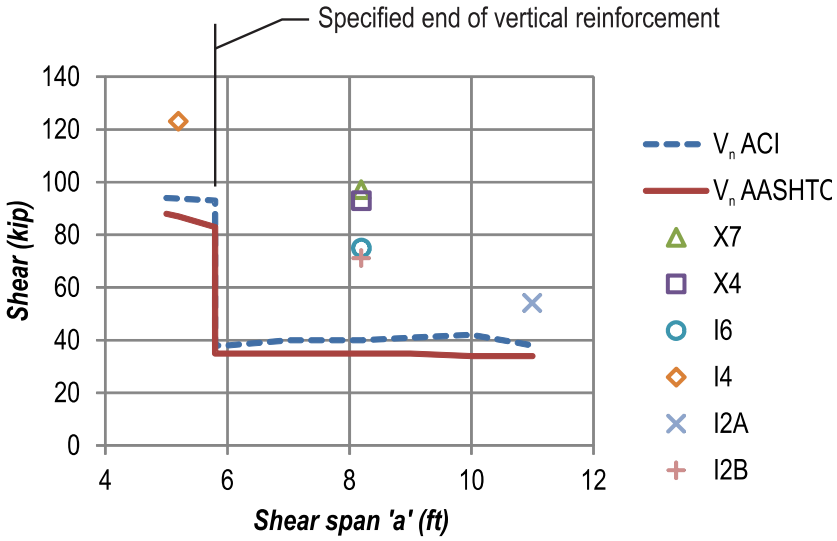

Figure 40–Experimental and theoretical shear capacities.

Table 3–Comparison of experimental and theoretical shear capacities.

	$V_{e\text{-}max}$ (kip)	V_n ACI (kip)	V_n AASHTO (kip)	$V_{e\text{-}max}/V_n$ ACI	$V_{e\text{-}max}/V_n$ AASHTO
X7	96	37	35	2.59	2.74
X4	94	37	35	2.54	2.69
I6	75	37	35	2.03	2.14
I4	123	94	87	1.31	1.41
I2A	54	38	34	1.42	1.59
I2B	71	38	35	1.87	2.03
Avg.				1.96	2.10
X only Avg.				2.56	2.71
I only Avg.				1.66	1.79

Table 4–Exterior girder shear strength considering contribution of barrier

	$V_{e\text{-}max}$ (kip)	Depth ratio (d*) exterior/interior	d* x V_n ACI (kip)	d* x V_n AASHTO (kip)	$V_{e\text{-}max}$ / (d* x V_n) ACI	$V_{e\text{-}max}$/ (d* x V_n) AASHTO
X7	96	1.4	52	49	1.85	1.96
X4	94	1.4	52	49	1.81	1.92
Avg.					1.83	1.94

The least conservative results came from girder I4, which was tested at a shear span of 2.1. This placed the critical section at the load point within the limits of the specified transverse reinforcement. As such, I4 was the only girder for which the nominal capacity included the contribution of shear reinforcement. Figure 36 shows that each of the inclined cracks in the shear span of girder I4 engaged transverse reinforcement, thus consideration of the reinforcement contribution is reasonable.

Experimental loads at the initiation of cracking provide another means of comparison with the theoretically calculated capacities. This comparison is useful for evaluating service behavior and cracking for similar in service girders. Figure 41 shows the theoretical concrete contribution as calculated by the ACI and AASHTO provisions. The theoretical concrete contribution represents the nominal strength of the standard section without shear reinforcement. The point data on this figure mark the total (dead plus superimposed) shear load of the first inclined cracking in the web. Load at first web cracking was determined from the strain gage data. Cracking load indicated by the strain gages was lower than the load at which cracking was visually observed. Data from Figure 41 are tabulated in Table 5. The average ratio of the experimental shear at cracking to the concrete contribution was 1.17 and 1.32 for the ACI and AASHTO procedures, respectively.

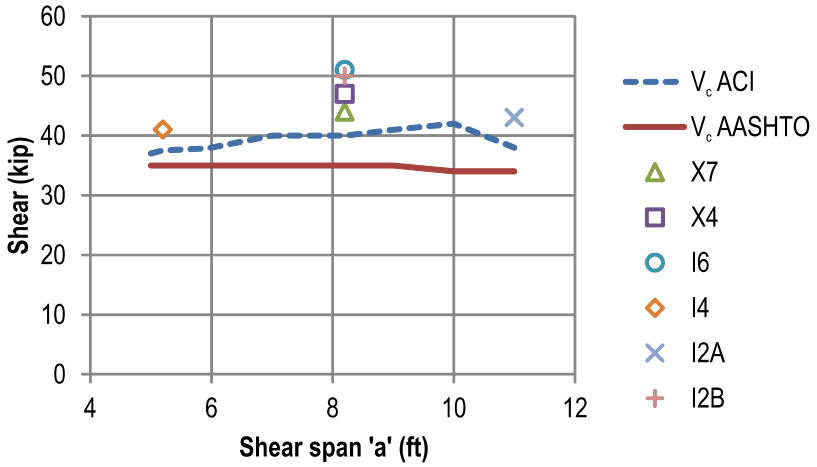

Figure 41–Shear at initial cracking and theoretical concrete contribution.

Table 5–Comparison of experimental and theoretical cracking shears.

	V_{cr-exp} (kip)	V_c ACI (kip)	V_c AASHTO (kip)	V_{cr-exp}/V_c ACI	V_{cr-exp}/V_c AASHTO
X7	44	40	35	1.10	1.26
X4	47	40	35	1.18	1.34
I2A	43	38	34	1.13	1.26
I2B	50	40	35	1.25	1.43
I4	41	37	35	1.11	1.17
I6	51	40	35	1.28	1.46
Avg.				1.17	1.32

Experimental moments and nominal moment capacities are summarized in Table 6. The theoretical moment capacities were calculated using the individual section properties from each test girder rather than from the properties of the standard section. A moment-curvature MathCAD worksheet developed by Consolazio et al. (2004) was used to calculate the theoretical moment capacity of the section. Calculations were rigorous, employing strain compatibility, equilibrium, nonlinear concrete stress-strain model (tension and compression), nonlinear steel stress-strain model for strands and mild steel, and biaxial bending.

Girder X4 was the only specimen to fail in flexure, with the experimental moment capacity being within 5% of the predicted capacity. During testing, crushing occurred in the extreme compression fibers of girder X4 at 2550 microstrain, confirming that girder was at or nearing flexural capacity. As none of the other girders failed in flexure, the experimental moments are less than the calculated moment capacities.

Table 6–Comparison of experimental moments and nominal moment capacities.

	M_{exp} (kip-ft)	M_n (kip-ft)	M_{exp}/M_n
X7	752	934	0.80
X4	745	782	0.95
I2A	572	693	0.83
I2B	560	675	0.83
I4	626	721	0.87
I6	585	743	0.79

6 Summary and Conclusions

Six pretensioned concrete girders were salvaged from an existing bridge and tested after nearly 55 years of service. Girders were tested in three point bending at a/d ratios from 2.1 to 4.5. A varying portion of the existing deck and/or curb was retained with each test girder. The experimental results were compared to theoretical predictions of strength capacity. Based on the experimental and analytical results, the following conclusions are made:

- Test girders behaved as tied arches at the latter stages of loading. This is evident from the relatively wide cracks which did not allow aggregate interlock and from the absence of transverse reinforcement necessary to allow truss action.
- Tied-arch behavior controlled the experimental strength of girders X7, X4 and I2A. Arches in these girders failed due to punching, flexural compression, and arch instability, respectively.
- For girders I2B, I4, and I6 the maximum load occurred just prior to the formation of an inclined crack in the web. These girders behaved as tied-arches during the latter stages of loading, however, their maximum capacities were limited by the capacity of the web to resist inclined cracking.
- The serviceability limit for girders tested at a/d ratios of 3.4 and less was formation of inclined cracks in the web. The thin 4 in. webs were culpable in the relatively small loads required to initiate web cracks.
- For tests at the same a/d ratio, the cast-in-place curb increased the average exterior girder strength by 30% over that of the interior girders with no curb.
- Nominal shear capacities calculated by ACI and AASHTO methods were conservative relative to the experimental results. On average ratio of calculated-to-experimental shear capacity was 2.0 for ACI calculations and 2.1 for AASHTO calculations.
- The concrete shear contribution, as calculated by ACI or AASHTO methods are recommended for estimating the cracking load of similar in-service girders. Concrete contribution as calculated by ACI and AASHTO methods were, respectively, 17% and 32% lower than the experimental cracking loads.

- End blocks effectively supported end region loads, preventing cracking in the end region in all but two tests, and strand slip in all but one test.
- Location and quantity of the transverse reinforcement in the test girders and the construction drawings. It is recommended that presence of vertical reinforcement be confirmed using non-destruction methods when analyzing the shear capacity of similar in-service girders. If the presence of transverse reinforcement is not verified, then it is recommended that shear contribution for the vertical steel be neglected.
- The experimentally determined prestress force in specimen I2A was 47% less than the specified initial prestress. The large difference between the specified and experimental values may indicate quality control issues in addition to higher than expected losses.
- In spite of relatively thin webs, small quantities of vertical reinforcement, and poor quality control during construction, the girders were able to support significant shear force after nearly 55 years of service.